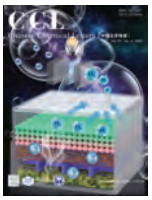
Chinese Chemical Letters 37 (2026) 112002

Contents lists available at ScienceDirect

Chinese Chemical Letters

journal homepage: www.elsevier.com/locate/cclet



Monochromophore-tunable supramolecular fluorescence-phosphorescence dual light-harvesting NIR emission for multi-dimensional information encryption

Siwei Wang[a], Fanxu Zeng[a], Yuan Yan[a], Jinghai Liu[a], Wei-Lei Zhou[a,b,*], Yong Chen[b,*]

[a] College of Chemistry and Material Science, The Technological Innovation Center of Supramolecular Chinese (Mongolian) Medicine, Innovation Team of Optical Functional Molecular Devices, Inner Mongolia Minzu University, Tongliao 028000, China
[b] College of Chemistry, State Key Laboratory of Elemento-Organic Chemistry Nankai University, Tianjin 300071, China

ARTICLE INFO

Article history:
Received 24 June 2025
Revised 10 October 2025
Accepted 21 October 2025
Available online 22 October 2025

Keywords:
Supramolecular assembly
Fluorescence-phosphorescence
Laponite
Light-harvesting
Multicolor luminescence

ABSTRACT

Organic fluorescence-phosphorescence dual-emitting materials based on tunable single chromophores have attracted much attention for their broad application prospects in information technology, display media and other fields due to their high luminescence stability, simple preparation process and excellent reproducibility. Herein, we constructed a novel LP-activated fluorescence-phosphorescence dual-light-harvesting (FPRET) supramolecular assembly based on LP with orthogonal charges, the phosphorescent molecule G and the NIR dye NIB through a supramolecular non-covalent strategy. The energy transfer efficiency of fluorescence is 54.68 % when the molar ratio of **G**/LP to NIB is 10:1, while the energy transfer efficiency and antenna effect of phosphorescence are 48.75 % and 241.43 respectively when the molar ratio of G/LP to NIB is 50:1. In addition, by co-assembling with carbon dots (CDs) and adjusting the ratio of donor to acceptor components, the full-color spectral regulation including white light (CIE chromaticity coordinates x, $y = 0.31$, 0.33) was realized. Utilizing this LP to promote the supramolecular full-color FPRET assembly of single fluorophore **G** and showing the multi-level anti-counterfeiting of intelligent logic gates through pattern, time, and color editing, it provides a new insight and direction for the development of a new generation of high-performance optical functional materials.

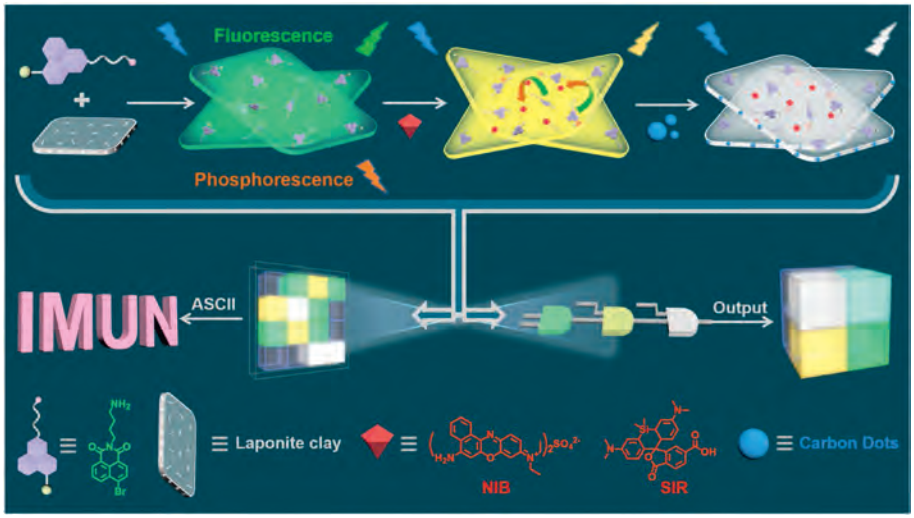
© 2026 Published by Elsevier B.V. on behalf of Chinese Chemical Society and Institute of Materia Medica, Chinese Academy of Medical Sciences.

In recent years, supramolecular luminescent materials based on host-guest multivalent interactions have been widely used in biological imaging [1–4], information encryption [5–7], sensing [8–11] and catalysis [12–14] due to their excellent luminescent properties and multi-stimuli-responsive capabilities, and have become one of the research hotspots in supramolecular science. The commonly used multi-charge host compounds cyclodextrin [15,16], cucurbit[*n*]uril [17–21] and macrocycle arenes [22,23] can not only change the assembly structure of guest molecules and promote their luminescent properties through the strong bonding ability of multivalent interactions, but also gather a variety of functional molecules in one at the same time and endow them with adjustable characteristics. For example, Wang *et al.*'s group [24] constructed a multivalent assembly based on carboxylated pillar[5]arene, quaternary ammonium tetraphenylethylene derivative (TPEDA), eosin Y (ESY) and Nile red (NR), which induced efficient energy transfer from guest TPEDA with AIE properties to ESY and then to NR for demonstrating the application in photocatalytic dehalogenation. Li *et al.* [25] reported a multivalent supramolecular light-harvesting assembly platform with excellent luminescence through the assembly of amphiphilic sulfocalix[4]arene and naphthyl 1,8-diphenylpyridinium derivatives, which was further co-assembled with Nile blue (NIB) to achieve efficient light-harvesting for showing near-infrared (NIR) imaging of C_6-ceramide in Golgi apparatus.

On the other hand, as a new type of intelligent luminescent material, fluorescent-phosphorescent dual emissive materials have shown exciting properties in display technology and other aspects [26–31], especially the single-luminophore system not only has high luminescence stability and excellent reproducibility, but also can emit light with a ratio change due to changes in external stimuli (including temperature, humidity) [32], which is suitable for constructing dynamic and reversible intelligent-response luminescent materials [33,34]. At the same time, the supramolecular light-harvesting system of resonance energy transfer (RET) can achieve long-wavelength near-infrared luminescence with large

* Corresponding authors.
E-mail addresses: zhouweilei_2011@163.com (W.-L. Zhou), chenyong@nankai.edu.cn (Y. Chen).

https://doi.org/10.1016/j.cclet.2025.112002
1001-8417/© 2026 Published by Elsevier B.V. on behalf of Chinese Chemical Society and Institute of Materia Medica, Chinese Academy of Medical Sciences.



Scheme 1. The illustration of the construction of the LP-activated fluorescence-phosphorescence dual-emission resonance energy transfer supramolecular assembly.

Stokes shift at a high donor/acceptor (D/A) ratio, and simplify the modification of complex covalently bonded fluorophores and give them controllability [35–39]. However, the light-harvesting of fluorescence-phosphorescence dual emission based on organic single chromophore is still a significant challenge.

Herein, we designed and synthesized an alkylamine-modified bromonaphthalimide derivative (**G**) as the guest molecule, and laponite (LP) with a unique propertie of negative surface charge and positive edge charge as the host compound [40,41]. Through a non-covalently activated supramolecular assembly method, combined with the dye NIB or silicon-based rhodamine (SIR), a near-infrared supramolecular light-harvesting system with efficient fluorescence-phosphorescence dual-emission resonance energy transfer (FPRET) of a single luminescent group in the aqueous phase was successfully developed. The electrostatic interaction between the negatively charged surface of LP and the positively charged **G** can limit the free rotation of **G** molecules and reduce non-radiative transitions, resulting in strong yellow-green fluorescence-phosphorescence dual emission. Interestingly, the secondary assembly with the dye NIB showed significant light-harvesting performance. The effective energy transfer efficiency at 525 nm was 54.68 %, and the effective energy transfer efficiency at 580 nm was 48.75 %, making it from 545 nm yellow-green light to 665 nm near-infrared light. For the dye SIR, the phosphorescence energy transfer efficiency can reach 91.72 %, and the luminescence is transferred to near-infrared light at 800 nm. Subsequently, the highly efficient fluorescent-phosphorescent dual-light harvesting supramolecular assembly was further assembled with negatively charged blue carbon dots (CDs). By adjusting the ratio of the donor/acceptor to CDs, full-color luminescence including white light (CIE chromaticity coordinates x, $y = 0.31, 0.33$) was obtained. This LP-promoted the FPRET supramolecular full-color assembly of single fluorophore **G** is conducive to the construction of intelligent logic gate multi-level anti-counterfeiting by tuning three parameters of pattern, time, and color, which provides new ideas and directions for the development of a new generation of high-performance optical functional materials (Scheme 1).

Firstly, the orange-red guest compound **G** (2-(4-aminobutyl)-6–bromo-1*H*-benzo[*de*]isoquinoline-1,3(2*H*)–dione) was obtained by adding excess 1,4-diaminobutane to the ethanol suspension of 4–bromo-1,8-naphthalic anhydride, refluxing for 24 h, cooling to room temperature and then vacuum filtration, with a yield of 67 % (Figs. S1–S3 in Supporting information). The **G** aqueous solution was prepared with 5 % DMF and 95 % water. The positively

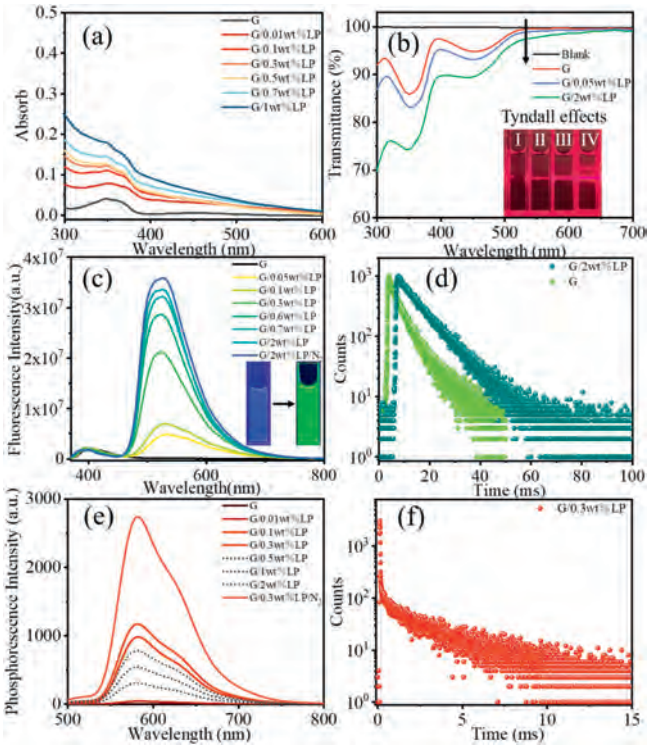


Fig. 1. (a) Absorption spectra of adding LP (from 0 wt% to 1 wt%) to **G** (0.01 mmol/L) in aqueous solution. (b) The optical transmittance with the LP into **G** (0.01 mmol/L). Inset: Tyndall effect of (I) water, (II) **G** and (III) **G**/0.05 wt% LP, (IV) **G**/2 wt% LP. (c) The phosphorescence spectra of **G** with LP (from 0 wt% to 2 wt%) in aqueous solution. (d) The fluorescence dynamic lifetime decay curves of **G**/LP at 525 nm at 298 K. (e) Phosphorescence emission spectra (delay 0.1 s) of **G**/LP in aqueous solution before and after N_2 bubbling at 298 K. (f) The photoluminescence dynamic lifetime decay curves of **G**/LP at 580 nm ([**G**] = 0.1 mmol/L, LP = 2 wt%, λ_{ex} = 350 nm, 298 K).

charged **G** is suitable for assembling with the negatively charged surface of LP, and the changes in the photophysical properties of the **G**/LP aqueous solution are studied by UV–vis absorption spectroscopy and photoluminescence spectroscopy. After adding LP into the **G** aqueous solution, the absorption intensity at 350 nm in UV–vis spectrum gradually increases with the gradual increase of LP (Fig. 1a). Meanwhile, the assembly process was monitored through the optical transmittance experiment. As shown in Fig. 1b, with pure water as the reference sample, the optical transmit-

tance of **G** and **G**/2 wt% LP shows slight changes. The optical transmittance of both decreases at 550 nm, and the Tyndall effect of **G**/2 wt% LP is more obvious than that of **G**. The changes in UV absorption and transmittance indicate that the electrostatic interaction between LP and **G**, as well as the hydrogen bonding and π-π stacking between **G** molecules, forms large nanostructured assemblies which may alter the electronic density distribution of **G** molecules, thereby changing their absorption. The alteration of the electronic density of **G** after the formation of the assemblies will also cause changes in its luminescent properties. Through the fluorescence spectrum (Fig. 1c), we found that the aqueous solution of **G** hardly emits light under 365 nm excitation, as LP was gradually added into **G** solution, an obvious fluorescence emission appears at 525 nm. With the increase of LP from 0.01 wt% to 2 wt%, the fluorescence lifetime of LP with 2 wt% almost reached the maximum value of 8.96 ns, and the fluorescence quantum yield reached 14.57 % (Figs. 1c and d, Figs. S6a, S6b, S7a and S7b in Supporting information). Interestingly, after adding LP to **G**, the phosphorescence spectrum shows an obvious emission peak at about 580 nm, which reaches the maximum at 0.3 wt% (Figs. 1e and f, Figs. S6c and S7c in Supporting information) with the lifetime of 3.25 ms, and the total quantum yield of 10.47 %. Meanwhile, through the comparison of N_2 experiments (Figs. 1c and e), there was almost no change in the fluorescence part, but the phosphorescence spectrum is greatly enhanced (due to the protection of the triplet excited state by N_2 from being quenched by dissolved oxygen), and the luminescence intensity is increased by 2.34 times, which further proves the appearance of 525 nm fluorescence and 580 nm phosphorescence dual emission of the assembly **G**/LP. When the content of LP exceeds 0.3 wt%, the phosphorescence at 580 nm may be quenched due to the competing interactions of excessive charges. Subsequently, in order to investigate the assembly mode of **G**/LP, the changes in morphology and zeta potential before and after the formation of the assembly were studied by transmission electron microscopy (TEM) and zeta potential experiments. The morphological changes of the assembly **G**/LP were shown by TEM, which ranged from nanofibers to numerous layered aggregates which further revealed the formation of the assembly (Fig. S4 in Supporting information). The zeta potential of the guest molecule **G** was measured to be 18.17 mV, indicating a positive charge. After assembly with the negatively charged host compound LP, the zeta potential increased from −44.34 mV of LP to −32.99 mV, suggesting that electrostatic interactions occur between the positively charged **G** and the negatively charged LP surfaces (Fig. S5 in Supporting information). The assembly was subsequently tested under four different conditions (Figs. S8-S10 in Supporting information), *i.e.*, temperature, pH, natural light exposure time, and solvent polarity (varying the DMF ratio in the solution). The results show that the natural light irradiation time has no effect on the fluorescence/phosphorescence of the assemblies. In addition, we also examined the spectral changes of the assembly **G**/LP under 365 nm ultraviolet light irradiation, and the luminescence intensity and the total quantum yield slightly decreased after 2 h irradiation under ultraviolet lamp. The change of temperature and pH has little effect on the fluorescence of the assembly, but has a certain effect on the phosphorescence of the assembly. However, different polarity has a certain effect on fluorescence and phosphorescence under different DMF ratios. As shown in Figs. S8-S10 (Supporting information), no obvious luminescence quenching phenomenon was observed under these four conditions, indicating that the assembly has satisfactory light stability. In the control experiment, negatively charged hyaluronic acid (HA) and sodium carboxymethyl cellulose (CMC) were added to the **G** aqueous solution; no significant changes in fluorescence-phosphorescence intensity were observed (Fig. S11 in Supporting information). In addition, before constructing **G**/LP assembly, compounds with the same charge as **G** were pre-added to LP, such as cationic cyclodextrin (β-CD$^+$), polyethyleneimine (PEI) and chitosan (CS) that the fluorescence and phosphorescence of **G**/LP were greatly inhibited (Fig. S12 in Supporting information). This was mainly because the negative charges on the LP were neutralized by the positively charged substances, thereby hindering the assembly of **G** with the LP. These experimental phenomena further prove that the non-covalent interaction between LP and **G** is primarily an electrostatic interaction, and the stacking effect of the rigid LP with orthogonal charges is more conducive to limiting the non-radiative transition of **G** molecules.

In view of the excellent fluorescent-phosphorescent dual emission performance and multi-charge platform in the aqueous phase of the assembly, it is beneficial to load the organic dyes with spectral matching through electrostatic interaction, and achieve efficient energy resonance transfer by shortening the distance to the acceptor fluorescent dyes. In this study, the UV–vis absorption of the near-infrared emitting dyes NIB or SIR shows a good spectral overlap with the emission peak of **G**/LP, ensuring the feasibility of energy transfer (Figs. 2a and d). Then the NIB or SIR was respectively selected as the acceptor, and the **G**/0.3 wt% LP assembly with strong phosphorescence emission as the donor. With the addition of NIB, the fluorescence and phosphorescence intensities of **G**/LP both showed a gradually decreasing trend under the excitation of 350 nm, while the luminescence intensity of NIB at 650 nm in either fluorescence or phosphorescence mode also exhibited a gradually increasing phenomenon (Figs. 2b and g). When the D/A ratio was 10:1, the fluorescence lifetime and fluorescence quantum yield at 525 nm decreased to 6.16 ns and 0.48 % respectively, while the lifetime at 650 nm of NIB increased by 1.5 times (from 1.80 ns to 2.70 ns), and the quantum yield increased by 2.5 times (from 1.73 % to 4.32 %) (Figs. S13-S15 in Supporting information). When the D/A ratio was 50:1, the phosphorescence lifetime and total quantum yield of **G**/LP at 580 nm respectively droped to 0.44 ms and 2.67 %, while the luminescence lifetime at 650 nm increased from 0.60 ms to 2.20 ms by 3.67 times, and the total quantum yield increased from 1.58 % to 9.04 % by 5.72 times (Figs. S16-S18 in Supporting information). These results indicate that this system not only achieves fluorescence energy resonance transfer from **G**/LP (donor) to NIB (acceptor), but also realizes triplet-to-singlet phosphorescence energy resonance transfer, resulting in delayed fluorescence of NIB. In addition, two main parameters, energy transfer efficiency (Φ_{ET}) and antenna effect (AE), are calculated to quantify and measure the effect of the system's light-harvesting. According to the luminescence quenching of **G**/LP/NIB during the energy transfer process, the fluorescence Φ_{ET} was calculated to be 54.68 %, while the phosphorescence Φ_{ET} and AE values are 48.75 % and 241.43 respectively at a D/A molar ratio of 10:1 (Figs. 2c and h, Fig. S22a in Supporting information). Furthermore, in order to investigate the universality of phosphorescence energy transfer in the assembly, we also selected the NIR emitting dye SIR as another acceptor. As SIR was gradually added to **G**/LP, the phosphorescence at 580 nm gradually weakened (the lifetime decreased from 3.18 ms to 1.48 ms; the total quantum yield decreased from 9.42 % to 3.74 %), while the emission peak at 690 nm gradually strengthened, along with the phosphorescence lifetime and the total quantum yield respectively increased by 6.45 times (from 0.22 ms to 1.42 ms) and by 10.15 times (from 1.11 % to 11.27 %) (Fig. 2e and Figs. S19-S21 in Supporting information). The Φ_{ET} reached 91.72 %, and the AE value reached 366.61 (Fig. 2f and Fig. S22b in Supporting information). In the control experiments, under the same conditions (350 nm excitation), no emission peaks were observed for NIB, SIR or LP/NIB, LP/SIR in the phosphorescence mode (Fig. S23 in Supporting information), and no phosphorescence emission was observed for the assembly **G**/LP under the maximum excitation of NIB (650 nm) or SIR (690 nm) (Figs. 2b and e). This further demonstrates that the assembly based

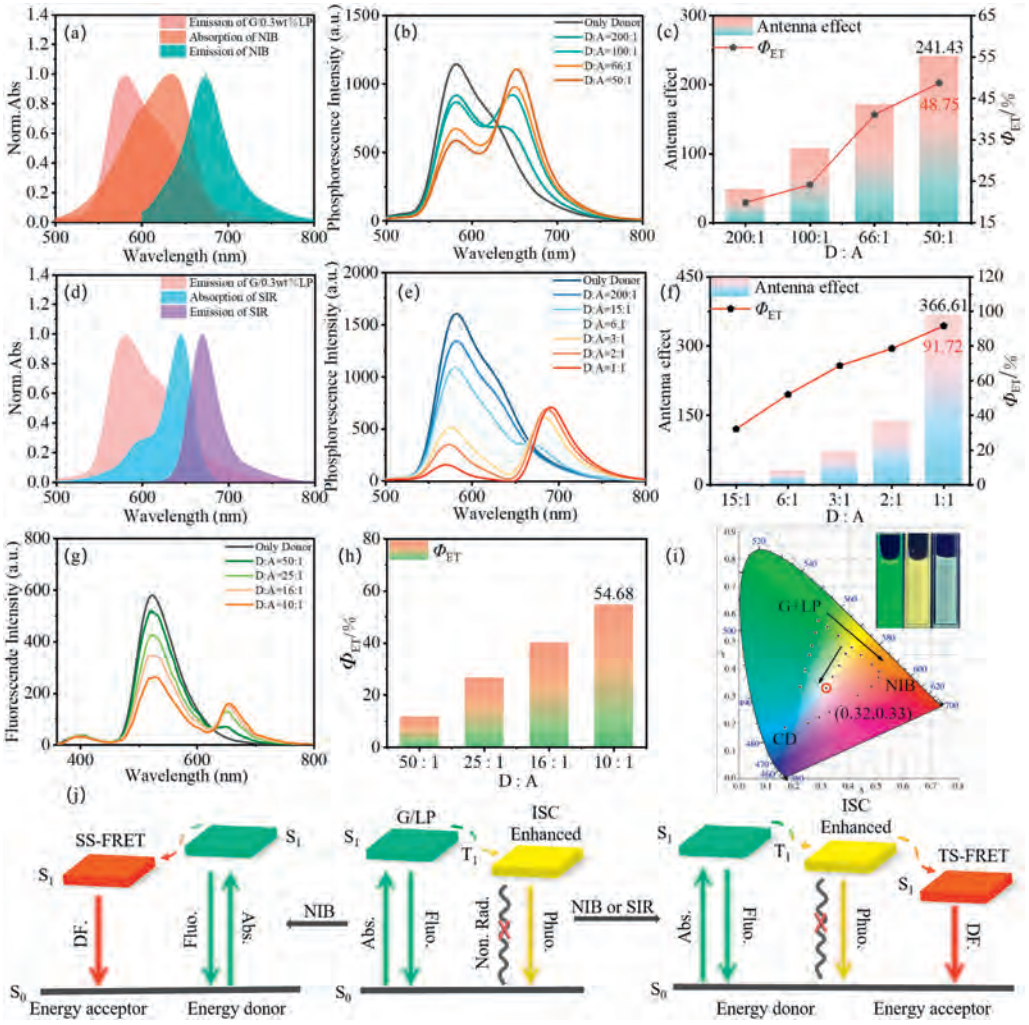


Fig. 2. Normalized emission spectrum of **G**/LP and the absorption and emission spectra of (a) NIB and (d) SIR. The phosphorescence spectrum (delayed by 0.1 s) of **G**/LP in aqueous solution with different concentrations of (b) NIB and (e) SIR. (g) The fluorescence spectrum of **G**/LP in aqueous solution with different concentrations of NIB. (c) The antenna effect/Φ_{ET} of **G**/LP in aqueous solution with different concentrations of NIB (according to emission of the donor: 580 nm, acceptor 1: 650 nm). (f) SIR (according to emission of the donor: 580 nm, acceptor 2: 690 nm). (h) Φ_{ET} of **G**/LP in aqueous solution with different concentrations of NIB (according to emission of the donor: 525 nm, acceptor: 650 nm). (i) CIE chromaticity diagram of corresponding the full-color luminescent coordinates in aqueous solution. (j) The graphical possible working mechanism of phosphorescence and fluorescence energy transfer process ([**G**] = 0.1 mmol/L, [NIB or SIR] = 1 mmol/L, LP = 0.3 wt%, λ_{ex} = 350 nm, 298 K).

on LP-promoted **G** fluorescence-phosphorescence dual emission can achieve fluorescence-phosphorescence dual energy resonance transfer (FPRET) with the NIR dye NIB or SIR. Multicolor luminescence has extensive applications in lighting and anti-counterfeiting fields, especially white emission. Considering the excellent FPRET of supramolecular assembly, we can achieve wide-spectrum output of multicolor photoluminescence by simply adjusting the molar ratio of D/A. After gradually adding NIB to the assembly **G**/LP, the luminescence of the solution gradually changed from green to orange. The same color change trend was also observed in the two-dimensional projection of the CIE (Commission Internationale de l'Eclairage) chromaticity diagram, from green (0.29, 0.58), to yellow (0.41, 0.48), and finally to orange (0.51, 0.39). Furthermore, carbon quantum dots (CD) with a large number of carboxyl groups on the surface (measured to have a zeta potential of −13.82 mV, Fig. S24a in Supporting information) could further assemble with the positively charged edges of the assembly **G**/LP. The fluorescence spectrum of CD under 365 nm excitation shows a clear emission peak around 455 nm, presenting blue luminescence (Fig. S24b in Supporting information). After the assembly of the host LP and CD, the fluorescence of CD was enhanced by 1.27 times, and the quantum yield increases by 2.03 times (Figs. S24b and S25-S27 in Supporting information). Therefore, the multi-level assembly combining LP/**G**, NIB and CD is conducive to the construction of multicolor tunable luminescence systems, especially featuring color fidelity and low color distortion for white light emission which has extensive applications in lighting and anti-counterfeiting. As shown in Fig. 2i, **G**/LP, **G**/LP/NIB and CDs respectively emit intense yellow-green, orange and blue light corresponding to the coordinates (0.29, 0.58), (0.51, 0.39) and (0.17, 0.19) in the CIE diagram. Interestingly, as the CD is gradually added to the yellow-emitting **G**/LP/NIB assembly, the emission of the assembly gradually approaches white emission and eventually reaches the white-light region, with the corresponding CIE coordinates (0.32, 0.33). For the white light emitting assembly, the stability test was carried out under four different conditions (temperature, pH, natural light irradiation time, polarity, Fig. S28 in Supporting information). The results show that temperature and natural light irradiation time have little effect on white light emission, pH and polarity have a certain effect on white light emission, but the overall stability is very good. Moreover, by adjusting the different proportions of **G**/LP, NIB and CD, full-color emission can be achieved (Fig. S29 in Supporting information), which is suitable for application in a security material. A possible mechanism is illustrated in Fig. 2j.

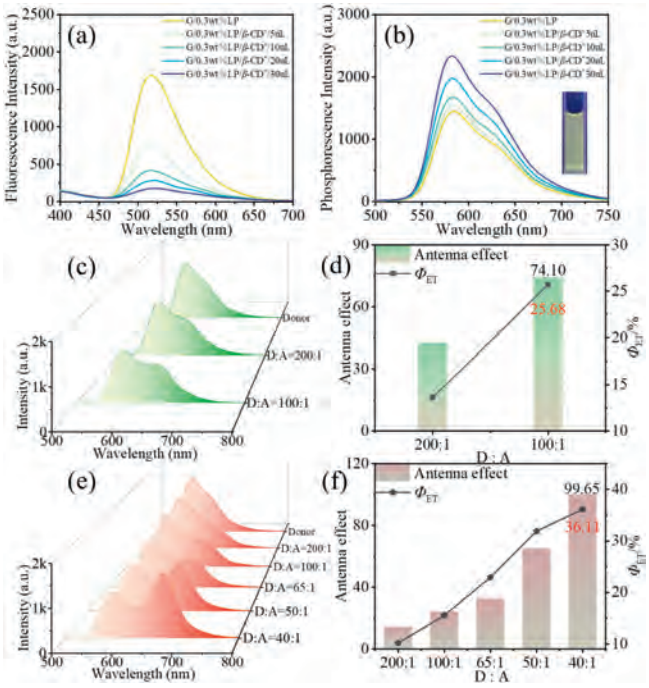


Fig. 3. (a) The fluorescence spectra and (b) the phosphorescence spectra (delay 0.1 s) of **G**/LP with β-CD$^+$ (from 5 μL to 30 μL) in aqueous solution. The phosphorescence spectrum (delayed by 0.1 s) of **G**/LP in aqueous solution with different concentrations of (c) NIB and (e) SIR. The AE/Φ_{ET} of **G**/LP in aqueous solution with different concentrations of (d) NIB (according to emission of the donor: 580 nm, acceptor 1: 650 nm) and (f) SIR (according to emission of the donor: 580 nm, acceptor 2: 690 nm). [**G**] = 0.1 mmol/L, [β-CD$^+$] = 100 mmol/L, [NIB or SIR] = 1 mmol/L, LP = 0.3 wt%, λ_{ex} = 350 nm, 298 K.

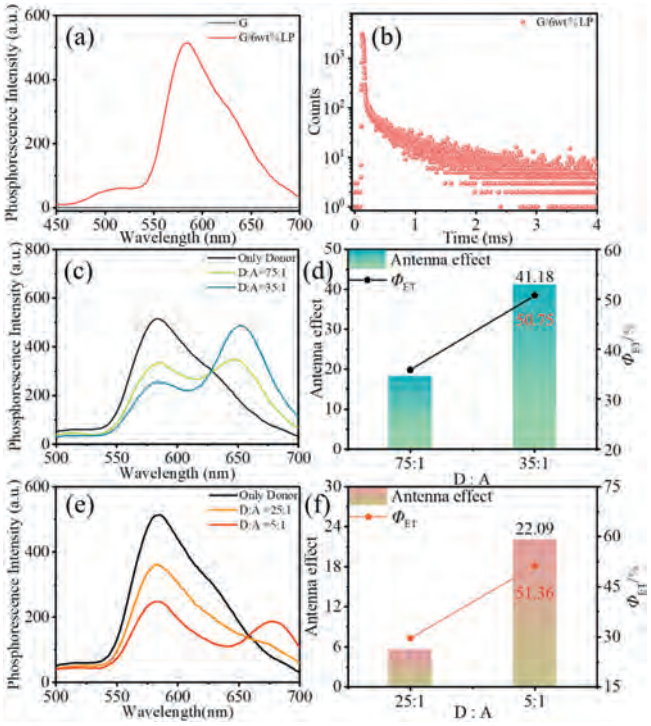


Fig. 4. (a) The phosphorescence spectra (delay 0.1 s) of **G**/LP in hydrogel. (b) The photoluminescence dynamic lifetime decay curves of **G**/LP at 580 nm. The phosphorescence spectrum (delayed by 0.1 s) of **G**/LP in aqueous solution with different concentrations of (c) NIB and (e) SIR. The antenna effect/Φ_{ET} of **G**/LP in hydrogel with different concentrations of (d) NIB (according to emission of the donor: 580 nm, acceptor 1: 650 nm). (f) SIR (according to emission of the donor: 580 nm, acceptor 2: 690 nm). [**G**] = 0.1 mmol/L, [NIB or SIR] = 1 mmol/L, LP = 0.3 wt%, λ_{ex} = 350 nm, 298 K.

The electrostatic interaction between the negative charge surface of LP and the positive charge **G**, the hydrogen bond and π-π stacking between **G** molecules, and the stacking between the rigid LP with orthogonal charges limit the non-radiative transition of **G** molecules, and reduce the collision with oxygen in water to a certain extent, which promotes the dual emission of fluorescence and phosphorescence. On the other hand, the remaining negatively charged surface in LP produces electrostatic interaction with cationic dyes, which shortens the distance between the donor and the acceptor for leading to efficient fluorescence-phosphorescence dual emission energy resonance transfer.

Amazingly, 0.3 wt% of the host compound LP was added to the guest **G** without complete dissolution and then the cationic cyclodextrins (β-CD$^+$) were added, most of the negative charges on the LP had already combined with β-CD$^+$, which to some extent hindered the combination with **G**. It was found that under these conditions that the fluorescence intensity quenching was weakened and the phosphorescence intensity was enhanced (Figs. 3a and b). The phosphorescence lifetime was increased to 3.65 ms and the total yield could be raised to 11.11 % (Figs. S30-S32 in Supporting information). However, after 3 min (when the LP was completely dissolved and fully assembled with **G**), the fluorescence intensity increased (Fig. S33 in Supporting information), and a rapid transition from fluorescence to phosphorescence and then back to fluorescence could be achieved, accompanied by a change in the emission color from weak green to yellow and then back to green. Meanwhile, we also used two positively-charged polymers, PEI and CS, to conduct the same tests. The same phenomenon was observed in these cases (Fig. S34 in Supporting information). This confirms that the occurrence of phosphorescence dynamic phenomena is due to the fact that β-CD$^+$ to some extent hinders the electrostatic binding interaction between LP and **G**. The fluorescence-phosphorescence switchable assembly **G**/0.3 wt%LP/β-CD$^+$ can also undergo phosphorescence resonance energy transfer with the NIB or SIR dyes. When the molar ratio of **G**/0.3 wt%LP/β-CD$^+$ to NIB is 100:1, the phosphorescence at 580 nm gradually weakens (the lifetime decreases from 3.35 ms to 3.03 ms, and the total quantum yield drops from 8.92 % to 6.70 %), while the emission peak at 650 nm gradually increases, with the phosphorescence lifetime enhanced by 1.55 times (from 1.40 ms to 2.17 ms) and the total quantum yield enhanced by 3.30 times (from 1.58 % to 5.21 %). The AE value is 74.10, and the energy transfer efficiency is 25.68 % (Figs. 3c and d, Figs. S35-S37 in Supporting information). When the molar ratio of **G**/0.3 wt% LP/β-CD$^+$ to SIR was 40:1, the phosphorescence at 580 nm gradually weakened (the lifetime decreased from 3.42 ms to 2.84 ms; the total quantum yield dropped from 9.42 % to 8.55 %), while the emission peak at 690 nm gradually increased, with the phosphorescence lifetime enhanced by 4.43 times (from 0.53 ms to 2.35 ms), and the total quantum yield enhanced by 2.90 times (from 1.11 % to 3.23 %). The AE value could reach 99.65, and the energy transfer efficiency was 36.11 % (Figs. 3e and f, Figs. S38-S40 in Supporting information).

Furthermore, when the LP content is increased to 6 wt%, the electrostatic interaction becomes stronger, resulting in a gel with a viscosity of 85 mpa (Figs. 4a and b). This state of the assembly can also undergo phosphorescent energy resonance transfer with NIB or SIR. The phosphorescence lifetime at 580 nm decreased from 1.12 ms to 0.22 ms and the total quantum yield decreased from 13.31 % to 7.68 %, as the molar ratio of **G**/6 wt%LP to NIB was 35:1. Simultaneously the lifetime at 650 nm increased by 2.6 times (0.17 ms increased to 0.45 ms) with the total quantum yield increasing by 8.5 times (1.50 % increased to 12.77 %) (Figs. 4c and d, Figs. S41-S43 in Supporting information) that the Φ_{ET} was 50.75 %, and the AE was 41.18 (Fig. 4d). Replacing dye SIR, the phosphorescence lifetime and total quantum yield at 580 nm decreased under

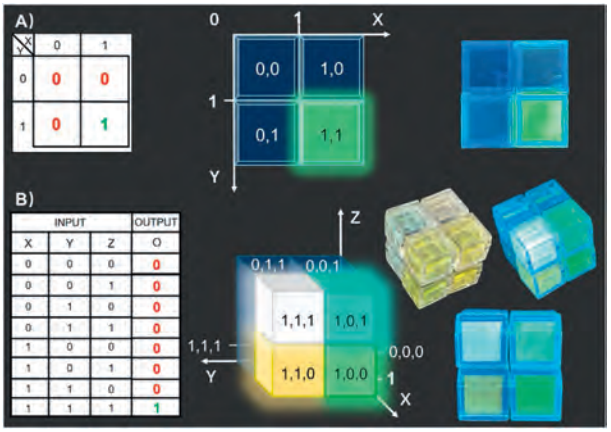


Fig. 5. Binary system table, schematic illustration, and chemical fluorescence AND gate for (A) binary inputs where X = **G**, Y = LP and (B) ternary inputs where X = **G**/LP, Y = NIB, Z = CD.

the 5:1 the molar ratio (from 1.12 ms to 0.48 ms, from 13.87 % to 12.30 %, respectively) while the lifetime and total quantum yield at 650 nm increased by 3.2 times (0.09 ms-0.29 ms) and 2.64 times (0.95 %−2.51 %), respectively (Figs. 4e and f, Figs. S44-S46 in Supporting information) (Φ_{ET}: 51.36 %, AE: 22.09).

3D color coding has attracted considerable scientific and industrial attention due to its superior information storage capacity compared to traditional scanning coding. The different spatial three-dimensional arrangements of colors convey different information. Taking advantage of the excellent hierarchical assembly characteristics of the assembly, it was designed as a binary logic (AND) gate intelligent optical system. When the "AND" gate performs logical operations, only when the input is a true value (1) will the corresponding spatial coordinate be added with the corresponding substance; if the input is a null value (0), the substance does not exist. And the logical truth value (1) is returned only when all the inputs are (1); When any input is null (0), its result is also null (0). In Fig. 5A, the two variables are guest **G** and the host LP. The output (1, 1) indicates that both exist to form an assembly **G**/LP, which exhibits bright green luminescence under ultraviolet light. Based on the previous step, we added two more variable information, thus obtaining a three-dimensional AND gate system. In Fig. 5B, X represents **G**/LP, Y represents NIB, and Z represents carbon quantum dots (CD). In this case, X is the first-level assembly input (1, 0, 0), emitting bright green. Only Y is added to X for cascade assembly, the coordinate becomes (1, 1, 0), resulting in bright yellow luminescence. After further introducing Z, white light emission is generated, which is the true value output (1, 1, 1). Through the hierarchical assembly of the assembly body, we designed a multi-level "AND" gate intelligent anti-counterfeiting system with regulated output.

Furthermore, on the porous plate (Fig. 6A), the host LP was added to **G** that bright green luminescent characters "1111" could be displayed under the irradiation of a 365 nm UV lamp. After adding the acceptor molecule NIB to the 2nd, 3rd, and 4th positions of the "1111" porous plate, bright green and yellow characters "2071" could be presented respectively. After continuing to add CD to the 3rd position, the luminescent characters "2025" (green, yellow, and white) were displayed respectively. Finally, by adding the excess NIB again, luminescent characters "8888" presenting red and pink colors could be obtained. Additionally, 16 small squares containing **G** solution are arranged into a 4×4 large square to encrypt and encode information based on the color changes over time. The specific color of each small square corresponds to a particular code or message, and can only be decoded when scanned under a 365 nm UV light. Initially, the **G** solution appeared pale

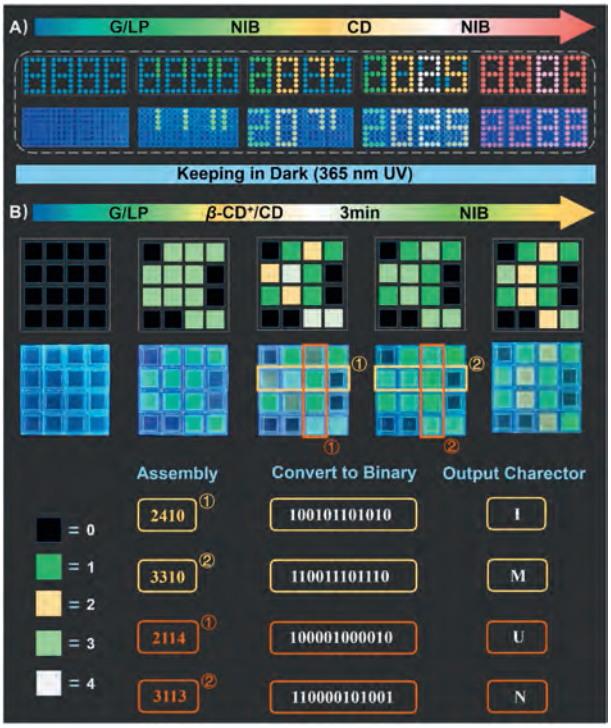


Fig. 6. (A) Photographs of multilevel information storage with supramolecular ink under 365 nm irradiation ([**G**] = 0.1 mmol/L, [LP] = 0.3 wt%, [NIB] = 1 mmol/L, CD = 100 mmol/L, λ_{ex} = 350 nm, 298 K). (B) Photographs of supramolecular dynamic anti-counterfeiting system under 350 nm irradiation ([**G**] = 0.1 mmol/L, [LP] = 0.3 wt%, [β-CD$^+$] = 100 mmol/L, NIB = 1 mmol/L, CD = 100 mmol/L).

yellow under the daylight, it did not emit light and appeared black under the UV light. Then LP was added at a specific position, and as it gradually dissolved, the solution turned weak green. At this time, we chose to add β-CD$^+$ at a specific position to hinder the assembly of LP and **G**, and the solution becomes yellow phosphorescence. On the basis of yellowing, we add CD to obtain white luminescence, as shown in Fig. 6B With the change of time, LP completely dissolves and yellow and white gradually becomes weak green, while LP completely dissolves and presents bright green without the addition of β-CD$^+$. Ultimately, the dye NIB can be added to the green luminescent solution to partially turn the solution yellow, thus making it impossible to read accurate information and achieving the purpose of destruction. Subsequently, these five colors are specified as five decimal numbers for encryption, black = 0, bright green = 1, yellow = 2, weak green = 3, and white = 4. The information obtained by the unique arrangement of decimal numbers can be binary converted, and the resulting binary codes are given different letters. The second line of yellow ① in Fig. 6B can be read as decimal "2410", converted to binary "100 101 101 010", and then read the information again to get the uppercase letter "I". As time changes, we can read the information of yellow ② as "3310", and also convert it to "110 011 101 110" and finally get the uppercase letter "M". Similarly, the uppercase letters "U" and "N" can be read in the third column of orange ① and ②, and the character of "IMUN" is finally deciphered.

In this work, a novel LP-activated fluorescence-phosphorescence dual light-harvesting supramolecular assembly was successfully constructed based on LP with orthogonal charge, phosphorescent molecule **G** and NIR dye NIB. Through supramolecular assembly method, the host compound LP assembled with the non-luminescent guest molecule **G** gave a dual emission of 525 nm fluorescence (lifetime: 8.96 ns) and 580 nm phosphorescence (lifetime: 3.25 ms). Subsequently, after cascade assembly with the dye NIB, an efficient FPRET of a single chromophore was achieved,

where the highest fluorescence energy transfer efficiency and phosphorescence energy transfer efficiency in the **G**/LP@NIB assembly were 54.68 % and 48.75 %, respectively. Thanks to the multivalent supramolecular platform, full-color luminescence including white light was obtained by changing the ratio of donor, acceptor and blue luminescent CD, and the conversion of phosphorescence-fluorescence was achieved by the competition of β-CD^{+}. This LP-promoted hierarchically tunable full-color supramolecular FPRET of single fluorophore **G** is a new way to construct the multi-functional anti-counterfeiting materials.

Declaration of competing interest

The authors declare that they have no known competing financial interests or personal relationships that could have appeared to influence the work reported in this paper.

CRediT authorship contribution statement

Siwei Wang: Writing – original draft. **Fanxu Zeng:** Data curation. **Yuan Yan:** Software. **Jinghai Liu:** Supervision. **Wei-Lei Zhou:** Writing – review & editing, Supervision, Funding acquisition, Data curation, Conceptualization. **Yong Chen:** Supervision, Conceptualization.

Acknowledgments

This work was supported by the National Natural Science Foundation of China (Nos. 22361036, 22571173), the China Postdoctoral Science Foundation (No. 2021M691661), Natural Science Foundation of Tianjin (No. 22JCYBJC00500) the Program for Youth Science and Technology Leading Talent of Inner Mongolia (No. GXKY25Z045), Inner Mongolia Natural Science Excellent Youth Foundation (No. 2025YQ050).

Supplementary materials

Supplementary material associated with this article can be found, in the online version, at doi:10.1016/j.cclet.2025.112002.

References

[1] S.S. Liew, Z. Zeng, P. Cheng, et al., J. Am. Chem. Soc. 143 (2021) 18827–18831.
[2] M. Zhang, J. Zhang, P. Alam, et al., Adv. Funct. Mater. 33 (2023) 2213927.
[3] A. Sailer, J.C. Meiring, C. Heise, et al., Angew. Chem. Int. Ed. 60 (2021) 23695–23704.
[4] J. Li, Y. Zhang, S. Liu, et al., Chin. Chem. Lett. 35 (2024) 109645.
[5] Y. Yang, A. Li, Y. Yang, et al., Angew. Chem. Int. Ed. 62 (2023) e202308848.
[6] Q. Wang, B. Lin, M. Chen, et al., Nat. Commun. 13 (2022) 4185.
[7] Y.J. Long, X.N. Han, Y. Han, et al., Chin. Chem. Lett. 36 (2025) 110600.
[8] M. Sun, S.L. Li, Q. Wang, et al., ACS Appl. Mater. Interfaces 16 (2024) 59327–59335.
[9] D. Wang, W. Li, W. Cheng, et al., J. Hazard. Mater. 464 (2024) 133015.
[10] A.J. Selinger, F. Hof, Angew. Chem. Int. Ed. 135 (2023) e202312407.
[11] W.L. Zhou, S. Wang, Y. Chen, Chin. Chem. Lett. 35 (2024) 109300.
[12] C.J. Haynes, L.K.S. Krbek, Nat. Chem. 14 (2022) 969–971.
[13] C. Wang, L. Xu, Z. Jia, et al., Chin. Chem. Lett. 35 (2024) 109075.
[14] R. Wang, Y. Liang, J. Rebek Jr., et al., Chin. Chem. Lett. 35 (2024) 109228.
[15] P. Liu, Chin. Chem. Lett. 36 (2025) 111406.
[16] I. Roy, J.F. Stoddart, Acc. Chem. Res. 54 (2021) 1440–1453.
[17] G. Song, B. Li, Z. Yang, et al., J. Am. Chem. Soc. 146 (2024) 25383–25393.
[18] C. Yin, Z.A. Yan, R. Yan, et al., Adv. Funct. Mater. 34 (2024) 2316008.
[19] L.L. Tan, M. Wei, L. Shang, et al., Adv. Funct. Mater. (2020) 2007277.
[20] Y. Xia, Y. Jiang, X.L. Ni, et al., Chin. Chem. Lett. 35 (2024) 109782.
[21] Y. Fan, J. Tan, C. Zou, et al., Chin. Chem. Lett. 36 (2025) 110101.
[22] Z. Wu, H. Qian, X. Li, et al., Chin. Chem. Lett. 35 (2024) 108829.
[23] X.N. Han, Y. Han, C.F. Chen, Chem. Soc. Rev. 52 (2023) 3265.
[24] M. Hao, G. Sun, M. Zuo, et al., Angew. Chem. 132 (2020) 10181–10186.
[25] X.M. Chen, Q. Cao, H. Krishna, et al., Angew. Chem. Int. Ed. 59 (2020) 10493–10497.
[26] R. Kabe, C. Adachi, Nature 550 (2017) 384–387.
[27] D. Li, F. Lu, J. Wang, et al., J. Am. Chem. Soc. 140 (2018) 1916–1923.
[28] X. Ma, J. Wang, H. Tian, Acc Chem. Res. 52 (2019) 738–748.
[29] H.T. Feng, J. Zeng, P.A. Yin, et al., Nat. Commun. 11 (2020) 2617.
[30] Z. Mao, Z. Yang, Y. Mu, et al., Angew. Chem. 127 (2015) 6368–6371.
[31] Y.Y. Hu, X.Y. Dai, X. Dong, et al., Angew. Chem. Int. Ed. 61 (2022) e202213097.
[32] Y. Yu, M. Si, W. Lu, et al., Chem. Eng. J. 478 (2023) 147271.
[33] Y. Wang, H. Wu, W. Hu, et al., Adv. Mater. 34 (2022) 2105405.
[34] X. Ma, M. Zhou, L. Jia, et al., Mater. Horiz. 10 (2023) 107–121.
[35] Q. Duan, Q. Zhang, J. Zhang, et al., Chin. Chem. Lett. 36 (2025) 111421.
[36] X.Y. Dai, M. Huo, Y. Liu, Nat. Rev. Chem. 7 (2023) 854–874.
[37] S. Wang, W.L. Zhou, Y. Chen, Chin. Chem. Lett. 35 (2024) 110261.
[38] Q. Zhang, X. Dong, F. Cui, et al., Chem. Commun. 60 (2024) 10064–10079.
[39] T. Xiao, X. Li, L. Zhang, et al., Chin. Chem. Lett. 35 (2024) 108618.
[40] S. Garain, B.C. Garain, M. Eswaramoorthy, et al., Angew. Chem. Int. Ed. 60 (2021) 19720.
[41] Y.G. Wu, W.L. Zhou, Y. Qiu, et al., Adv. Sci. 12 (2025) 2415418.